Progress Towards a Quantum Dot Photovoltaic:

Nanocrystal Deposition on Structured Titanium Dioxide Nanotubes

Kevin Emmett

Physics Senior Thesis

Advisor: Dr. Sandra Rosenthal

April 2008

1. Introduction and Motivation

Faced with the prospect of depleting oil supplies,[1] and the almost certainty of global climate change,[4] we are compelled to seek alternative sources to supply our growing energy demand. Several clean energy technologies will play an important role in this challenge, including wind, geothermal, biomass, hydroelectric, and nuclear. However, none of these technologies has the scalable capacity to meet the whole of our global energy demands.[6] For that, we must look to the sun. The sun provides power to the earth at a rate of 130 TW. Current global energy consumption is at a rate of 14 TW.[7] In just one hour, the sun provides enough power to supply our energy needs for an entire year. Tapping into this vast quantity of energy represents a grand challenge of scientific research and engineering. Current silicon technologies have thus far experienced limited deployment, primarily due materials costs. Developing novel methods of capturing solar energy is required. Here, semiconductor nanocrystals may play an important role. Properties of these small crystals may prove useful in developing alternative photovoltaic architectures. This thesis describes the application of semiconductor nanocrystals into a novel photovoltaic device structure, and recent progress towards realizing this device. The two principle areas of experimental work were fabrication of a nanostructured TiO_2 thin film, and deposition of nanocrystals onto the TiO_2 surface. To provide background, we begin with a summary of the relevant aspects of nanocrystal physics.

2. Semiconductor Nanocrystals

Research in the Rosenthal lab is centered on understanding the physical and chemical properties of semiconductor nanocrystals. Nanocrystals, or quantum dots, are

crystalline semiconductors on a size scale from one to ten nanometers. They are currently a subject of intense research activity targeting a wide range of potential applications, including light emitting diodes (LEDs),[8-10] photovoltaics,[11-14] single-electron transistors,[15] and fluorescent tags for biological imaging.[16-18] The utility of nanocrystals lies in their unique size-dependent optical and electronic properties, chiefly a size-tunable optical absorption and emission spectra. Nanocrystals of various sizes, and their associated absorption spectra, are depicted in Figure 1.

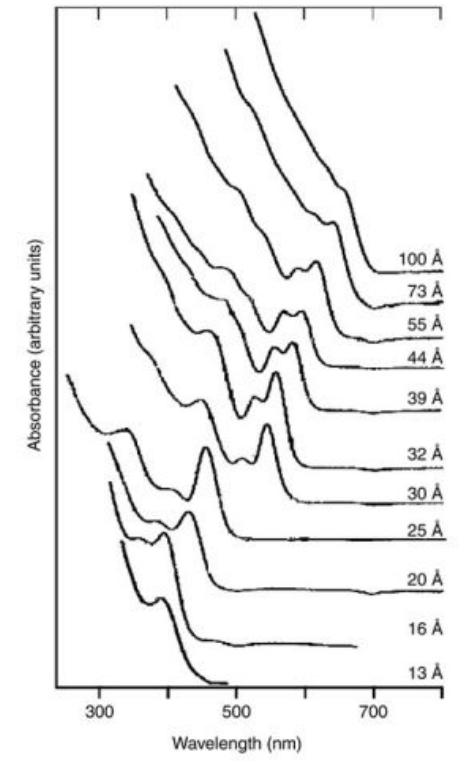

Figure 1. Top: Absorption spectra for several sizes of CdSe nanocrystals. Bottom: Nanocrystals as synthesized.[3]

Nanocrystals exist in the size regime between bulk material and individual molecules. This has important consequences for the electronic structure of the system.[19] A molecule is characterized by well defined orbitals; electronic transitions can only occur between these discrete energy levels. In contrast, bulk material is characterized by continuous energy bands that arise from the splitting of degenerate orbital states. A nanocrystal is not sufficiently large for the bulk band structure to form completely, thus is characterized by discrete electronic transitions, however the energy of these transitions is dependent on the size of the nanocrystal. The

nanocrystal retains the principle feature of semiconductor band structure: a fully occupied valence band, and an unoccupied conduction band.

Size-dependent effects in nanocrystals can be understood in terms of quantum confinement of free charge carriers. In a semiconductor, generation of free charge typically depends on excitation of a bound electron in the valence band into the conduction band by absorption of an energy greater than the band gap of the material, leading to a delocalized electron and hole within the system. A second possibility, upon absorption of an energy slightly lower than the band gap energy, is the formation of a quasiparticle state in which the electron is locally bound to a hole in the valence band. In this case, the negative electron will orbit the positive hole, much like a hydrogen atom. This quasiparticle state is known as an exciton. In all semiconductors, an exciton will have a characteristic radius between electron and hole, known as the bulk Bohr radius. For CdSe, the nanocrystal used in this research, the bulk Bohr radius is 5.6 nm.[20]

Confinement occurs when a dimension of the system is reduced below the exciton radius. Here, dimension refers to the spatial degrees of freedom within the system. A nanocrystal is a zero-dimensional system; free charge carriers are confined all three spatial dimensions. At this size scale, there is not enough volume in the crystal for the exciton to form, and the electron and hole exist as free charge carriers. At this point the properties of the nanocrystal become strongly size dependent.

As previously mentioned, one of the most remarkable facts about nanocrystals is the size dependence of the optical absorption and emission spectra. There exists a simple model for qualitatively understanding this behavior. This model, originally developed by

Brus,[21, 22] treats a free charge in the nanocrystal as a particle in an infinite spherical potential well. The Hamiltonian for this system is given by

$$\hat{\mathrm{H}} = -\frac{h^2}{8\pi^2 m_c}\nabla_c^2 + \hat{\mathrm{V}}$$

Solution of the Schrödinger equation for this Hamiltonian yields a series of discrete energy levels inversely proportional to the radius of the potential well, *R*, given by

$$E_n = \frac{h^2 n^2}{8 m_c R^2}$$

This accounts for the experimental observation of increasing transition energy with decreasing nanocrystal size. A more thorough treatment includes a term for the Coulomb attraction between electron and hole, and a term for the polarization of the crystal due to the presence of a point charge; however the qualitative behavior is the same.[3] With an understanding of the basic physics of nanocrystals, we now turn to photovoltaics, first describing the traditional cell and then addressing how nanocrystals may be used for increased efficiency.

3. Photovoltaics

The principal goal of this project was the application of semiconductor nanocrystals into a proposed photovoltaic device structure. In this section, the traditional silicon photovoltaic will be described, and the major sources of efficiency loss will be identified. An alternative device structure incorporating semiconductor nanocrystals will be described.

The operating principle behind all solar cells is the photovoltaic effect. Solar energy, in the form of photons, is incident on semiconducting material. The absorption of

photons with energy in excess of the band gap energy drives the excitation of free electrons into the conduction band. When separated by a potential, these electrons will flow freely through the material, producing an induced photocurrent which can be used to power a load.

3.1. Traditional Photovoltaics

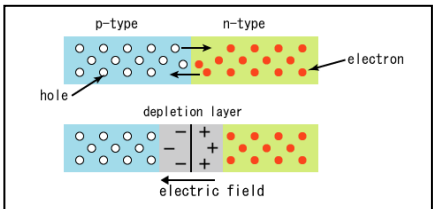

Figure 2. A *pn*-junction

The photovoltaic response of a traditional silicon solar cell is due to the effect of the *pn*-junction. When *n*-type silicon, typically doped with phosphorus, is diffused into *p*-type silicon, typically doped with boron, a planar interface is formed between the two regions. Excess electrons in the *n*-region, driven by a difference in chemical potential, will diffuse across the interface, recombining with holes in the *p*-region, resulting in a net positive charge in the *n*-region, and a net negative charge in the *p*-region. A potential difference is established between the two sides, opposing further diffusion of majority carriers. This region is called the *depletion region*, due to the depletion of mobile carriers. A diagram of a *pn*-junction is provided in Figure 2. When a photon is absorbed within the depletion region, the generated electron-hole pair is separated by the force of the electric field. Once separated, the free carriers drift through material and are collected at an electrode, yielding a photocurrent through an external path.[23]

The silicon solar cell has two major sources of efficiency loss: (1) Carrier recombination in the bulk material. Free charge carriers generated outside the photoactive region immediately recombine in the material, and do not contribute to the photocurrent.

Even when free carriers are generated, there is still a possibility of recombination with minority carriers in the bulk material. The thicker the layer is, the higher the probability of recombination. (2) Thermal losses. When a photon is absorbed, only one exciton is generated. Any energy in excess of the band gap energy is lost as heat. Thus the conversion efficiency of a *pn*-junction solar cell is band gap dependent. Thermodynamic assumptions have placed an ideal limit of 29% on silicon photovoltaics, and 44% for the optimal band gap of 1.1 eV.[24] While it should be theoretically possible to generate an exciton for each multiple of the band gap energy, in bulk material this process is exceedingly inefficient.

Significant limitations exist on the performance of traditional photovoltaics, and new paradigms are needed. Numerous alternatives to the traditional silicon photovoltaic design have been proposed, for example *pn*-heterojunction, thin film, and organic polymer photovoltaics. The use of nanostructured materials presents a compelling alternative. Our ability to engineer structures at the nanoscale provides us with the ability to fine tune the properties necessary for improved performance. A number of properties of nanocrystals make them an ideal candidate for a novel photovoltaic device, which will now be detailed.

3.2. Nanostructured Photovoltaics

One of the more promising alternatives to silicon photovoltaic technology is the Grätzel cell.[25] The Grätzel cell is an electrochemical cell consisting of a matrix of porous, nanocrystalline TiO_2 deposited on the surface of a transparent conducting oxide (TCO). The TiO_2 nanoparticles are sensitized with an organic dye, typically Ru-based, and the

matrix is infiltrated with a hole conducting electrolyte. The photoactive dye molecules generate electron-hole pairs upon absorption of light, and the electron is transported to the TiO_2, where it is collected at an electrode and used to power a load. Donation of an electron from a redox couple in the electrolyte returns the dye to its ground state.[26]

Power conversion efficiencies of the Grätzel cell have exceeded 10%,[27] making the Grätzel cell competitive with existing commercial technologies. The high efficiency of this architecture is due to two features: (1) an increased photoactive region due to the porous TiO_2 surface; and (2) the separation of charge generation from charge transport, reducing carrier recombination of photogenerated charges. By immediately transporting the electron into the TiO_2, the chance for it to recombine with the generated hole is minimized. The low charge recombination rate has led to internal photon-to-electron conversion efficiencies greater than 80%.[27] Unfortunately, widespread deployment has been hindered by stability problems stemming from leakage of the liquid electrolyte, limiting the useful lifespan of the system. To avoid this difficulty, all solid-state designs have been proposed, for example organic, flexible polymer layers. However, current conversion efficiencies for these devices remain low.[28]

A number of studies have demonstrated that nanocrystals can be effectively sensitized onto the surface of TiO_2,[29, 30] leading to the suggestion that they may be used as a light harvesting element, in place of the organic dye.[31, 32]

Our solar cell architecture builds on the Grätzel cell by using CdSe nanocrystals as light harvester and indium tin oxide (ITO) as a hole conducting layer. In place of a disordered matrix of TiO_2 nanoparticles, a highly ordered TiO_2 thin film is used. This is partly due to the lager size of the CdSe nanocrystals, compared with organic dyes, and

partly because it is believed the structured TiO_2 will improve vectorial charge transport and mobility of collected electrons. A diagram of the device structure, and the associated energy band diagram, is provided in Figure 3.

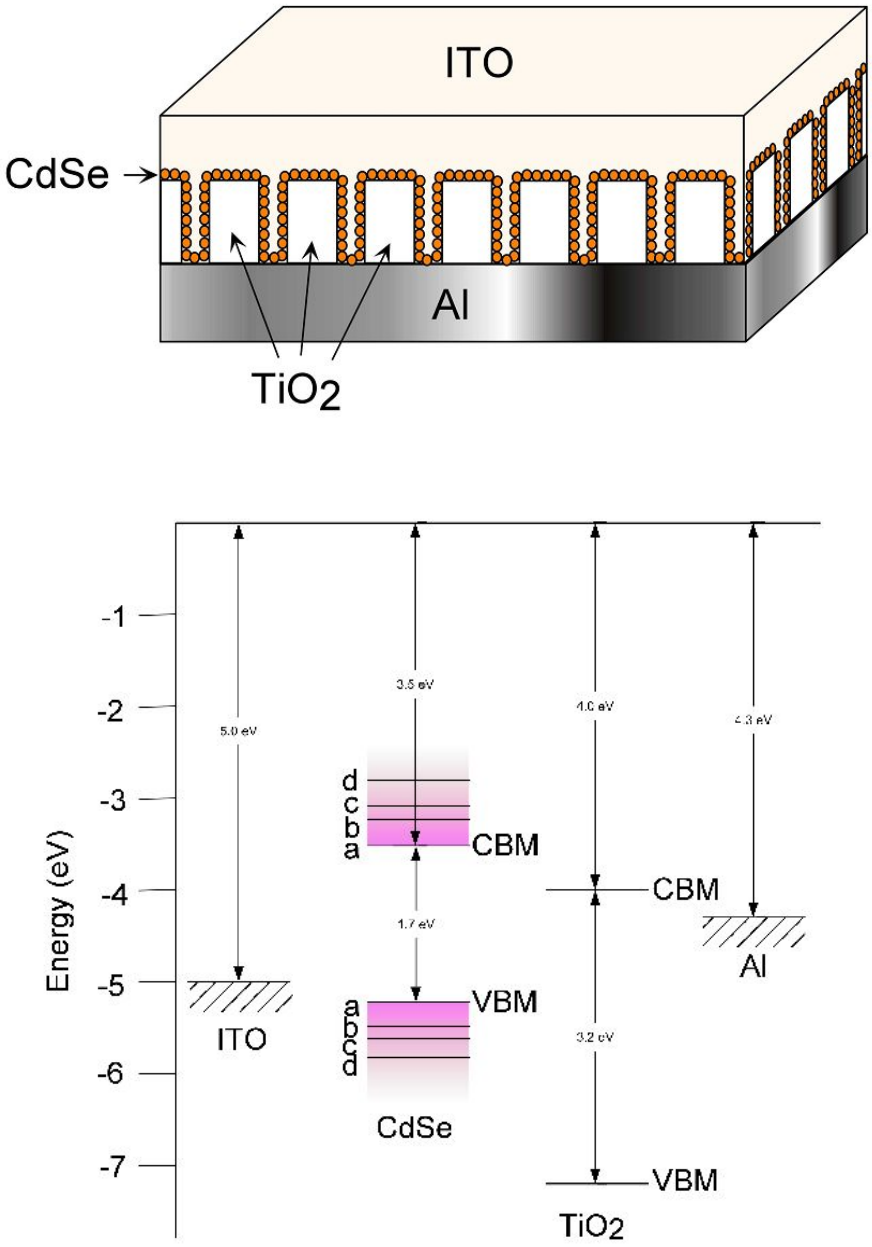

Figure 3. Top: Diagram of a nanocrystal-sensitized solar cell. CdSe coat the walls of a nanostructured TiO_2 thin film. Bottom: Energy band diagram for the above cell. Both images due to Laura Swafford.[5]

Nanocrystals offer a number of advantages over organic dyes. First, they are inorganic and highly robust. Second, their larger size acts to form a barrier between the TiO_2 electron conducting layer, and the ITO hole conducting layer, minimizing charge recombination. Third, they absorb a broader portion of the solar spectrum than dye molecules. Because CdSe is the most well understood nanocrystal system, it has been used in our current device designs. Future devices may implement PbSe nanocrystals, as it absorbs an even broader range of the solar spectrum (see Figure 4). Finally, there has been a significant amount of excitement recently over the possibility of multiple exciton generation, that is, through the process of impact ionization more than one free electron generated per input photon. One report, Schaller *et al*. has demonstrated the generation of seven excitons from a single photon.[14] Vast improvements in efficiency are foreseeable if the incident photon to electron conversion ratio can be increased.

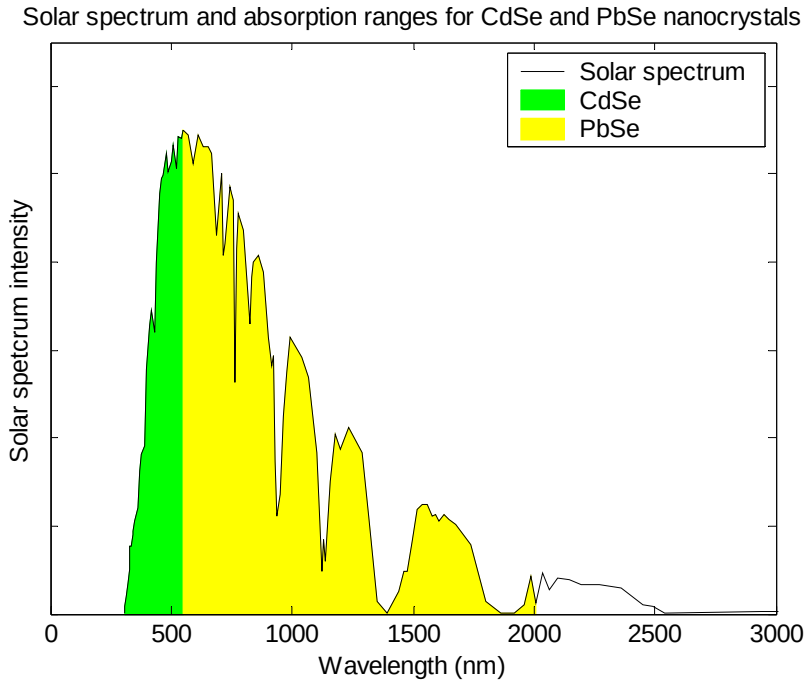

Figure 4. CdSe and PbSe matched to the solar spectrum

4. Nanostructured TiO_2 Thin Films

The bulk of this research project centered on the fabrication of highly-ordered, nanostructured TiO_2 thin films to serve as the electron conducting layer in a nanocrystal solar cell. Building on earlier work in the group using an alumina-template embossing method, an alternative approach employing the electrochemical anodization of titanium thin films was attempted. This method was successfully employed to fabricate large-area arrays of high quality, vertically-oriented TiO_2 nanotubes.

4.1. Previous Work: Alumina-Template Embossing

Previous work in the Rosenthal group directed at fabricating structured TiO_2 layers was focused on an alumina-template embossing procedure developed by Goh *et al.*[2] The procedure is outlined in Figure 5. Poly-(methyl methacrylate) (PMMA) is drop cast onto an alumina template with a 50 nm pore diameter. The sample is heated to 200 °C to infuse the polymer into the pores. A backing layer of poly(dimethylsiloxane) (PDMS) is coated onto the PMMA layer and allowed to cure at room temperature. A wet chemical etch then separates the polymer layer from the alumina foil. A thin film of sol-gel TiO_2 is then spin-cast onto an ITO-glass slide. Immediately after spin-casting, the polymer layer is pressed onto the TiO_2 film, embossing pores into the film. The polymer layer is removed, and the sample is annealed to crystallize.

While this method is capable of producing pores of uniform diameter with consistent distribution, it suffers from a number of drawbacks. First, the technique is difficult. An intermediate polymer layer is required to transfer the pores from alumina to titania. Numerous points in the process can degrade the quality of the polymer film.

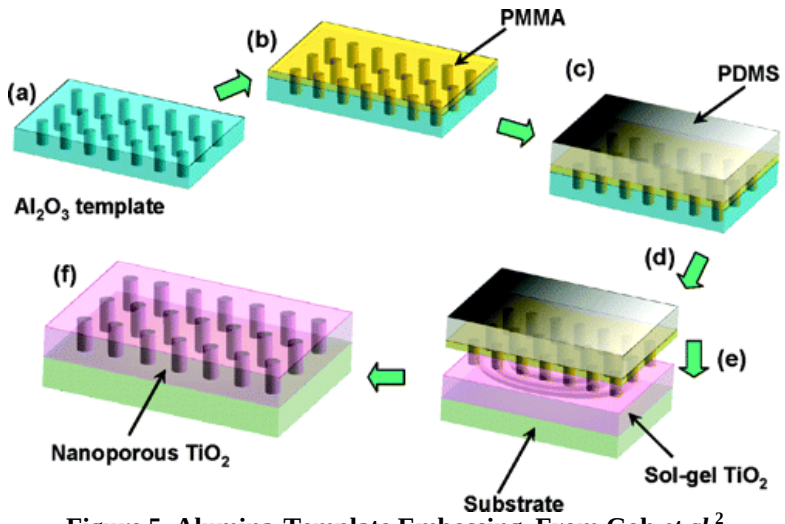

Figure 5. Alumina-Template Embossing. From Goh *et al.*[2]

Second, the surface coverage of pores on the TiO_2 film is poor, as can be seen from the image. The creation of pores is a result of embossing by the polymer layer, and differences in applied pressure can drastically affect the resulting film quality. Third, the scale of the technique is limited by the size of the alumina template, and would likely be difficult to scale up. The largest surface coverage achieved using this method has been ~0.25 cm^2. Fourth, the technique offers no control over the morphology of the resulting pores and is entirely limited by the morphology of the alumina template. Pore diameters of 50 nm may be too small to allow for deep penetration by nanocrystals. These drawbacks pointed toward the need for an alternative method of fabricating a nanostructured TiO_2 electrode.

4.2. Potentiostatic Titanium Dioxide Anodization

Anodization of titanium in a fluorine containing electrolyte has been shown to result in a vertically-oriented array of TiO_2 nanotubes.[33-36] TiO_2 nanotubes formed in this way have been researched for a variety of applications, including water photoelectrolysis,[37] photocatalysis,[38] and gas sensing.[39] From the perspective of

photovoltaic device design, the anodization method offers several advantages over alumina-template embossing. First, it is simpler. Formation of the nanotube array is self-assembled, single-step process. Second, the anodization results in uniform surface coverage. Third, control of the anodization parameters allows control of the resulting film morphology: tube length, pore diameter, and wall thickness. Additionally, there appears to be no limit on the overall nanotube length. In 2007, Prakasam *et al*. used the method to form a self-standing, 720 μm thick TiO_2 nanotube layer, starting with a titanium foil only 250 μm thick![40] We now turn to a detailed description of the experimental procedures followed.

5. Experimental Methods

5.1. Nanocrystal Synthesis

A number of techniques exist for fabricating nanocrystals, including molecular beam epitaxy (MBE), chemical vapor deposition (CVD), ion implantation, and wet chemical synthesis. In this project, CdSe nanocrystals were fabricated via the high temperature pyrolysis of organometallic precursors, a procedure due to Murray *et al*.[41] This colloidal, bottom-up synthesis is advantageous for its relative simplicity and the uniform size distribution of the resulting nanocrystals.[42]

The pyrolysis method is outlined in Figure 6. First, the selenium complex is formed by dissolving 0.96-g Se powder (Aldrich, 99.999%) in 100 mL of tributylphosphine (TBP, Aldrich, 90%). Next, the cadmium complex is formed by mixing the following chemicals in a three-neck flask: 0.257-g Cadmium Oxide (CdO, Strem, 99.99%), 6.0-g trioctylphosphine oxide (TOPO, Aldrich, tech grade 90%+), 4.0-g

hexadecyl amine (HDA, Aldrich, 90%), and 1.0-g dodecylphosphonic acid (DDPA, in-house synthesis). The solution is heated under argon purge using a thermal mantle to 150 °C, then brought to 330 °C under passive argon. The solution is vigorously stirred until cadmium phosphonate is formed and the solution turns clear. Once clear, the temperature is reduced to 260 °C, and 10 mL of the Se:TBP solution is injected into the flask, initiating nanocrystal growth. Initial growth is rapid for the first few minutes, slowing down over the next twenty minutes. The nanocrystals are allowed to grow to the desired size, and then cooled under argon to stop the growth process. To determine the nanocrystal size, a small amount of solution is pulled from the flask. An absorption spectrum is taken with a Cary 50 Bio UV-Visible Spectrophotometer, and major absorption features are compared with literature values.[43]

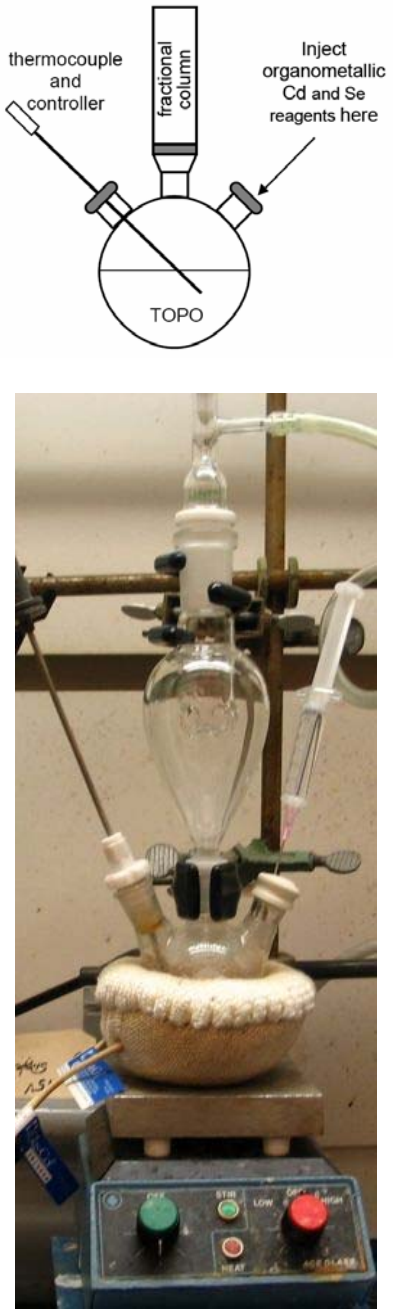

Figure 6. Top: Diagram of apparatus. Bottom: A photograph of the experimental setup.

Once the desired size is achieved, a cleanup procedure is performed to recover the nanocrystals. The pot solution is transferred to vials, diluted with methanol and centrifuged at 4500 rpm for 3 minutes to precipitate the nanocrystals. The liquid is discarded and the vial filled with one inch hexanol and centrifuged at 4500 rpm for 30 minutes. This cleanup

process is repeated as many times as necessary, however nanocrystals are lost with each cycle. As synthesized, this preparation yields CdSe nanocrystals with surface cadmium atoms passivated by TOPO, HDA, and DDPA. The nanocrystals are stored in solution, typically dissolved in either hexanes or toluene. Pyrolytically synthesized CdSe nanocrystals, with an average size of 4.5 nm, dissolved in hexanes, were used in the following experiments.

5.2. TiO_2 Nanotube Array Fabrication

Titanium foils, 250 μm thick, were obtained from Sigma-Aldrich and cut to 6.25 cm^2. Prior to anodization, the samples were degreased by sonicating in 2-propanol and acetone. Anodizations were performed in a specially designed etch cell, depicted in Figure 7. The cell consists of a square Teflon base and bowl shaped cell chamber. At the base of the cell chamber is a small hole. Using a rubber O-ring to seal the connection, the titanium foil was placed directly underneath the hole. A thin piece of copper is used as a back electrode. A platinum wire, bent into a spiral, acts as a counter electrode. The wire is held in place by a brass support ring. The copper anode and platinum cathode were connected to a Keithley 2400 source meter, interfaced with an Apple G3 running custom LabView software to monitor anodization current. The anodization is started and stopped automatically in LabView. To prevent contamination of the electrolyte, the anodization must be performed in a fume hood.

Electrolyte solutions contained either Potassium Fluoride (KF, Sigma-Aldrich, 99%) or Ammonium Fluoride (NH_4F, Sigma-Aldrich, 98%). Sonication was typically

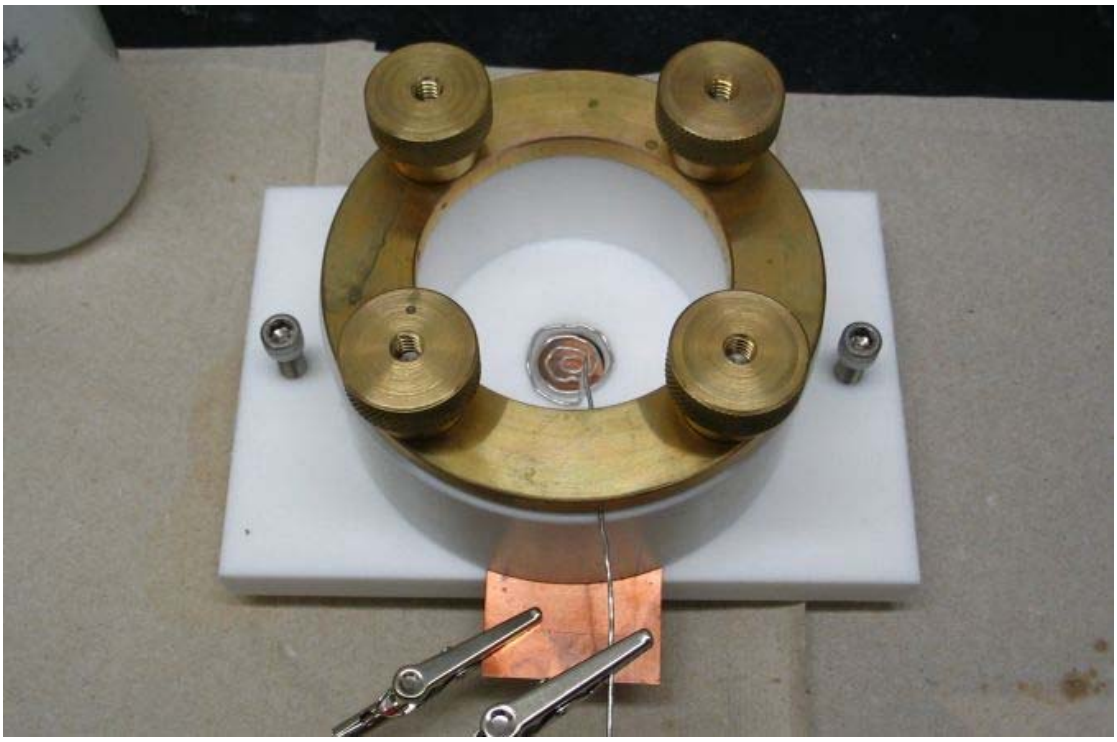

Figure 7. The anodization etch cell

required to form a solution. Organic-based solutions used either ethylene glycol (Fischer, 99.8%) or formamide (Fischer, 99.8%) as a solvent.

After the anodization is completed, the sample is removed from the etch cell. The sample is rinsed in ethanol and deionized water, and dried under a nitrogen stream. As fabricated, the nanotubes are amorphous TiO_2. To crystallize into anatase- TiO_2, the sample is annealed in atmosphere at 450 °C for 5 hrs, with 3 hr ramp times (2.5 °C/min).

5.3. Nanocrystal Deposition

The second phase of the project was to attach nanocrystals to the surface of the TiO_2 nanotube array. Three methods were attempted: drop casting and immersion, chemical linking, and electrophoretic deposition.

5.3.1. Drop Cast and Immersion

Two simple methods were tried to initially test nanocrystals deposition: First, a small amount of nanocrystal solution was drop cast onto the sample by pipette. Second, samples were allowed to sit immersed in a dilute nanocrystal solution for a period of time ranging from 6 to 48 hours. After each procedure, the sample was rinsed with toluene to remove loose nanocrystals.

5.3.2. Chemical Linking

Chemical linking is a well established technique of using a bifunctional linker molecule (HOOC-R-SH) to attach CdSe and CdS nanocrystals to the surface of a TiO_2 substrate.[30, 44] The TiO_2 is strongly attracted to the carboxylate group, while the thiol group binds strongly to the CdSe nanocrystal. An outline of the process is provided in Figure 8.

Mercaptopropionic Acid (MPA) (HOOC-CH_2-CH_2-SH) was used as a linker

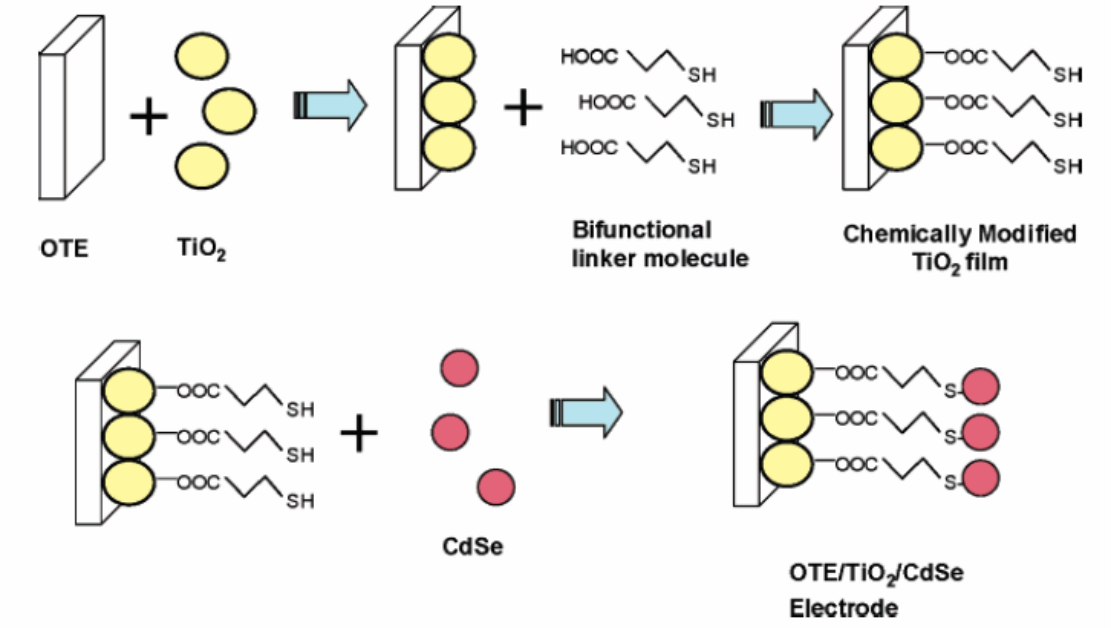

Figure 8. An outline of the chemical linking process. From Goh *et al.*[2]

molecule to successfully bind CdSe to the TiO_2 nanotube arrays. A solution of 10 vol% MPA in acetonitrile was prepared. Anodized TiO_2 samples were immersed in the solution for between 4 and 24 hrs. After immersion, the electrodes were rinsed thoroughly in acetonitrile to remove loose MPA, and then immersed in dilute nanocrystal solutions of varying optical density for between 12 and 96 hrs. Finally, the samples were rinsed in toluene to remove loose nanocrystals.

5.3.3. Electrophoretic Deposition

Electrophoretic Deposition is a straightforward application of an electrochemical cell. Two electrodes are immersed in a bath containing a dilute solution of nanocrystals in a non-polar solvent. At room temperature, some of the nanocrystals will be thermally charged.[45] When a voltage is applied between the two electrodes, the nanocrystals migrate under the influence of the electric field towards either electrode. Once they reach the electrode, the nanocrystals become bound to the surface, most likely through Van der Walls attraction.[46] The experimental setup is depicted in Figure 9.

Figure 9. EPD experimental setup

CdSe nanocrystals, dissolved in hexanes, were deposited onto TiO_2 nanotube arrays under a driving potential of 500 Volts. The experiment was run under a nitrogen atmosphere to minimize evaporation of the solvent. Standard deposition time was 15

minutes. After completing the deposition, the electrodes were removed from solution and held in air for 5 minutes, allowing the nanocrystal film to anneal.

5.3.4. Imaging and Characterization

Several instruments were used to characterize the nanotube films. For measurements of pore diameter and wall thickness, as well as analysis of film quality, a Hitachi S-4200 Scanning Electron Microscope (SEM) was used. This has recently been superseded by a Raith eLINE SEM, which is capable of imaging at a much higher resolution. Data using this device was not available while writing this thesis. An SEM works by collecting the secondary electrons scattered when a sample is exposed to a high-energy electron beam (15 keV).[47] Generally, an SEM is best at imaging features on a scale 10-1000 nm, and thus proved very useful for imaging nanotube arrays with features on the order of 100 nm.

Higher resolution images, as well as crystallographic and composition information, was obtained using a Philips CM20 Transmission Electron Microscope (TEM). The principle of TEM is the detection of electrons transmitted through a specimen when subject to a high-energy electron beam (400 keV).[48] TEM was used to characterize nanotube quality and verify nanocrystal deposition. For the purposes of this project, the resolving power of the TEM was generally more than necessary for basic characterization.

Two complementary methods were used to measure nanotube length. One was the mechanical fracturing of the sample prior to SEM imaging. Fracturing dislodged planes of the array and allowed a profile view of the layer to be imaged (see Figure 14). From this, the approximate nanotube length could be determined. The second method was to

remove the nanotube layer entirely, generally by scraping away the layer. A Veeco Dektak profilometer was then used to measure the step height difference between the anodized and unanodized section of titanium foil.

Elemental composition, important for verifying nanocrystal deposition, was determined using Rutherford Backscattering Spectroscopy (RBS) and Energy Dispersive X-Ray Spectroscopy (EDS). RBS is a technique whereby high energy alpha particles are incident on a sample surface. Analysis of the energy of backscattered ions can be used for elemental analysis.[49] Vanderbilt operates a 1.8 MeV van de Graaff accelerator for use in RBS analysis. EDS is an extension of SEM functionality. A high-energy electron beam is incident on a substrate, exciting atoms on the surface. X-rays emitted from the relaxation of these atoms can be measured to obtain a unique signature of the elements present in the sample.

6. Results and Discussion

6.1. Anodization Results

Nanostructured TiO_2 thin films have been successfully fabricated, and are vastly superior to earlier templating techniques. See Figure 10 for a comparison. The nanotube films offer uniform coverage over a larger area compared to the template films.

The characteristics of the nanotube morphology, namely nanotube length, pore diameter, and wall thickness, can be controlled by varying the anodization parameters, chiefly anodization voltage, anodization duration, and electrolyte solution. Of these, the electrolyte solution has the strongest influence on nanotube morphology. Anodization voltage must then be chosen within a narrow range to allow for nanotube growth.

Features of the nanotube morphology cannot be controlled independently; when a parameter is adjusted it will change all aspects of the nanotube array. It was observed that nanotube pore diameter responds strongly to anodization voltage. Wall thickness varies as well, but no clear trend was identified.

Figure 10. Top: Alumina-Template Sample. Bottom: Anodized Sample.

Anodizations were performed using both aqueous and organic electrolytes. Aqueous electrolytes have the advantage of requiring a lower anodization voltage and less time, however the quality of the resulting nanotube array is poorer than that of an organic electrolyte. The standard aqueous electrolyte consisted of 0.1 mol KF and 1.0 mol H_2SO_4 in water. See Table 1 for a list of aqueous anodization conditions, and resulting nanotube characteristics. Note no measurements of nanotube length were performed for aqueous samples. An SEM image of a characteristic nanotube array fabricated in an aqueous electrolyte is provided in Figure 11.

	Anodization Parameters		Nanotube Morphology	
Sample	Voltage (V)	Time (hr)	Pore Diameter (nm)	Wall Thickness (nm)
1	10	1	46	15
2	15	1	68	13
3	20	1	78	15

Table 1. Representative anodization results for an aqueous electrolyte

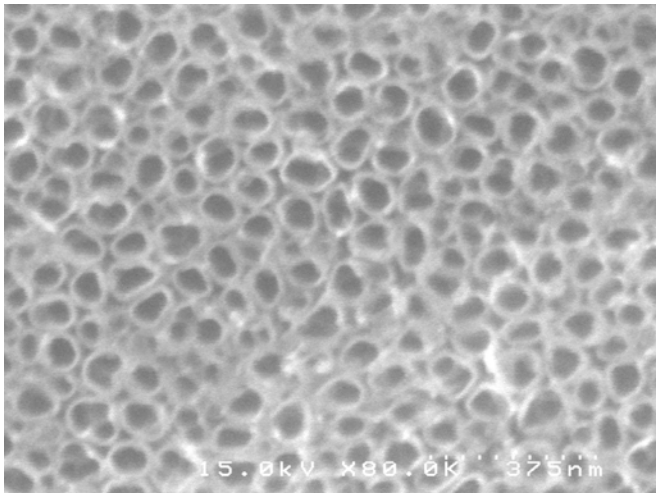

Figure 11. Anodized nanotubes in aqueous electrolyte.

Organic electrolytes proved to be more robust and allow for longer nanotube growth than the aqueous electrolytes. The standard organic electrolyte consisted of 0.25 wt% NH_4F in ethylene glycol. See Table 2 for a list of organic electrolyte conditions, and the resulting nanotube morphology. A series of SEM images is provided in Figure 12. TEM images are provided in Figure 13. Profile views are seen in Figure 14.

The viscosity of the organic electrolyte acts to counter the motion of the fluorine ions in solution, slowing the etch process down. Hence organic etches require much longer amounts of time; however this yields nanotube films of much more uniform quality.

	Anodization Parameters		Nanotube Morphology		
Sample	Voltage (V)	Time (hr)	Tube Length (μm)	Pore Diameter (nm)	Wall Thickness (nm)
1	40	14	15	72	10
2	50	14	18	90	10
3	60	14	15	129	8

Table 2. Representative anodization results for an organic electrolyte

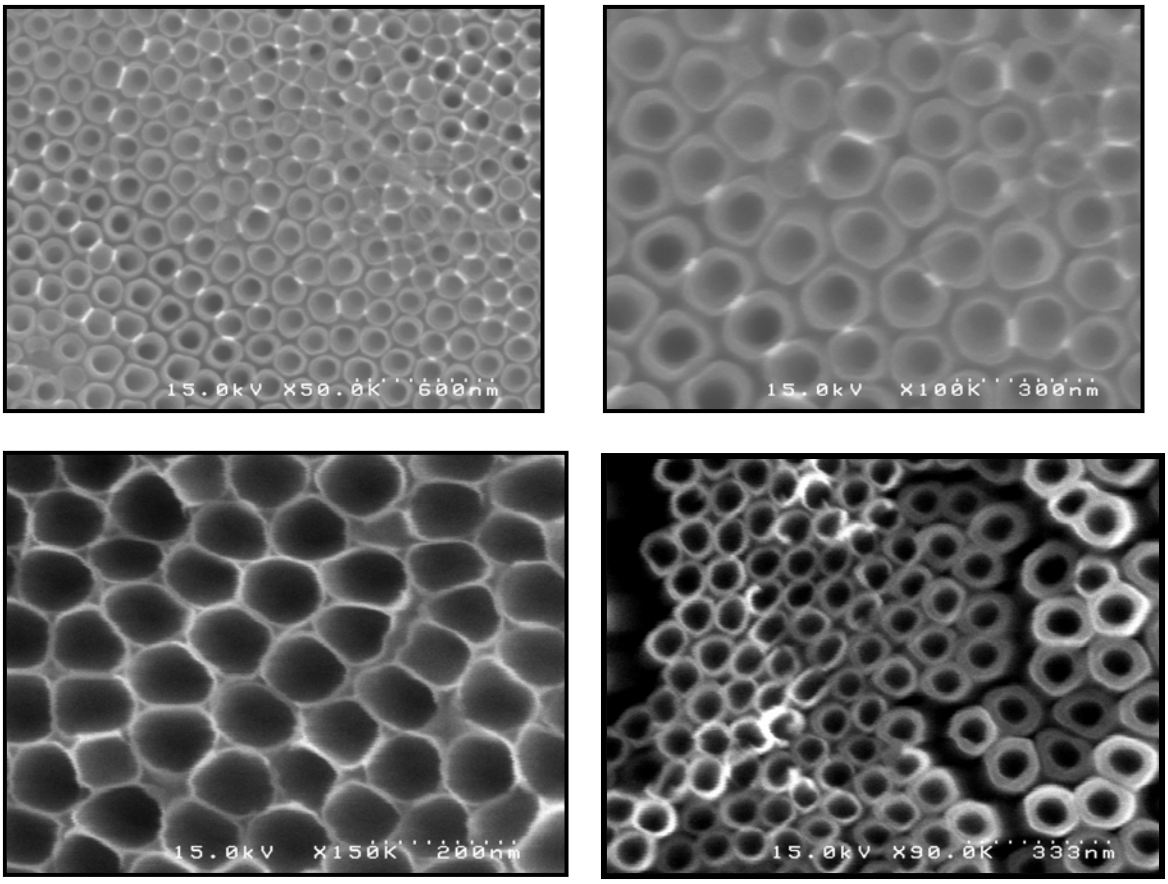

Figure 12. A sample of anodized nanotube arrays formed in organic electrolyte (0.25 wt% NH_4F in ethylene glycol)

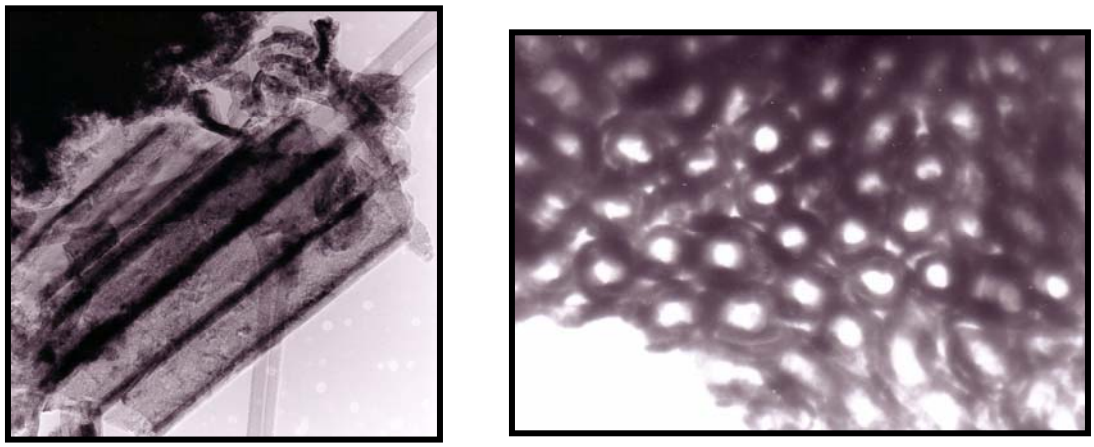

Figure 13. TEM images of nanotube arrays. Sonication to prepare for TEM destroys most of the array, however clumps of tubes remain together.

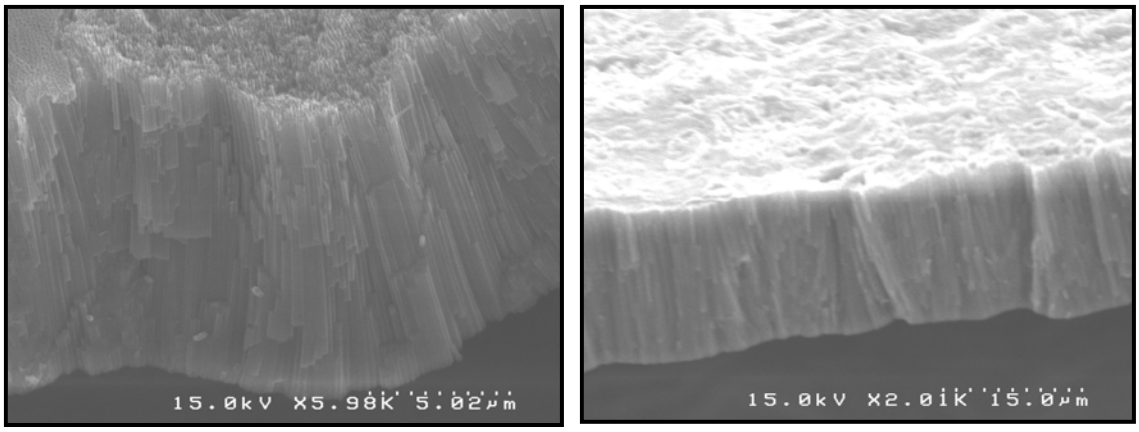

Figure 14. Profile views of nanotube arrays used to measure nanotube length.

6.2. Anodization Mechanics

The anodic formation of TiO_2 nanotubes is similar to that of anodic alumina. Competing processes at the metal-oxide interface and oxide-electrolyte interface reach a steady state, while chemical etching initiates the formation of pores. Pores, and the voids between them, form at an equal rate, yielding nanotubes. This discussion of anodization mechanics is primarily due to Grimes *et al*.[50]

When the anodizing potential is applied, oxygen ions (O^{2-}) in the electrolyte migrate under the influence of the electric field towards the titanium anode, where they interact with titanium ions (Ti^{4+}) to build up an initial oxide layer at the metal surface. The surface oxidation reactions for an aqueous electrolyte can be represented as:

$$H_2O \rightarrow O_2 + 4e^- + 4H^+$$

$$Ti + O_2 \rightarrow TiO_2$$

As the oxide layer grows, polarization of the Ti–O bond leads to a uniform field-assisted dissolution of the oxide layer. The Ti^{4+} ions dissolve into the electrolyte, while the O^{2-} ions move towards the metal-oxide interface. In this way, the oxide layer continues to grow. Localized pits at the oxide layer surface form as a result of chemical interaction

with the acidic electrolyte. These sites serve as pore forming centers. The reaction can be represented as:

$$TiO_2 + 6F^- + 4H^+ \rightarrow TiF_6^{2-} + 2H_2O$$

Within these pits, the shallower oxide layer will cause an increase in the field-assisted dissolution, causing the pits to grow and form pores. The chemical dissolution is the key to nanotube growth, as it maintains localized field-assisted dissolution at the pore bottoms, allowing the tubes to grow in length. Eventually, a steady-state is reached where oxide growth at the oxide-metal interface is exactly balanced by oxide dissolution at the oxide-electrolyte interface.

6.3. Thin Film Anodization

As described, the anodization is incompatible with the device structure we envision. By anodizing a titanium foil, the nanotube array is bound to the bottom layer of titanium. No attempts at removing the layer have been successful. The nanotube layer is too fragile to exist in self-standing form, and fractures when removed. A device implementation would require the deposition of a transparent hole-conducting polymer layer. However, current polymers have conductivities that are too low to be useful in a solar cell device.

Anodization of thin films of titanium, between 300-400 nm and deposited via RF-sputtering onto FTO coated glass slides, has been reported.[51] The anodization is monitored and stopped when the titanium layer has been completely anodized. When annealed, the nanotube layer turns transparent. This approach would allow light to enter

through the glass side. This approach was attempted, however has currently been unsuccessful.

300 nm layers of titanium were deposited onto an ITO coated glass slide via e-beam deposition. Anodization was attempted using standard parameters for an organic electrolyte. It was observed that within minutes of the voltage being applied, the titanium layer had been completely etched away. Examination in the SEM showed patchy regions of TiO_2, and no evidence of nanotubes.

A potential reason for the failure of the anodization is that in the early stages of the etch, field-assisted oxide formation and dissolution dominate over them chemically-assisted pore formation and growth. If the initial titanium layer is too thin, the metal layer may oxidize and dissolve before the chemical etch has time to take hold. The deposition of thicker layers of titanium would prevent this problem; however properties of titanium make traditional methods of deposition difficult. Alternatively, by reducing the applied potential, it should be possible to slow the formation of the oxide layer and reduce the field-assisted dissolution, allowing the pore formation process time to begin. These experiments are currently in process.

6.4. Nanocrystal Deposition

Of the three deposition techniques attempted, chemical linking proved to be the most robust; however electrophoretic deposition presents a promising alternative. Neither drop casting nor immersion was successful in linking nanocrystals to pore walls.

6.4.1. Drop Cast & Immersion

Sample fluorescence indicated nanocrystal deposition onto the surface. However, when the samples were scraped into a 2-propanol solution and sonicated to prepare for TEM imaging, the nanocrystals, evidenced by their fluorescence, settled at the bottom of the solution. This indicates that both drop cast and immersion do not result in a nanocrystal layer binding to the surface of the TiO_2 substrate. A method to functionalize the surface and actively bind the nanocrystals is necessary.

6.4.2. Chemical Linking

RBS data indicates successful deposition, see Figure 15. TEM imaging shows nanocrystals linked to the inner surface of the nanotubes, further confirming successful deposition (Figure 16).

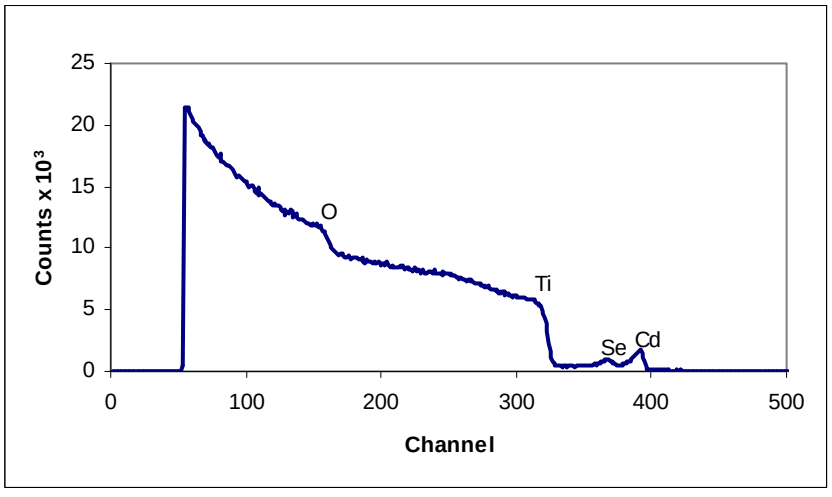

Figure 15. RBS of Chemically Linked NC+ TiO_2 NT

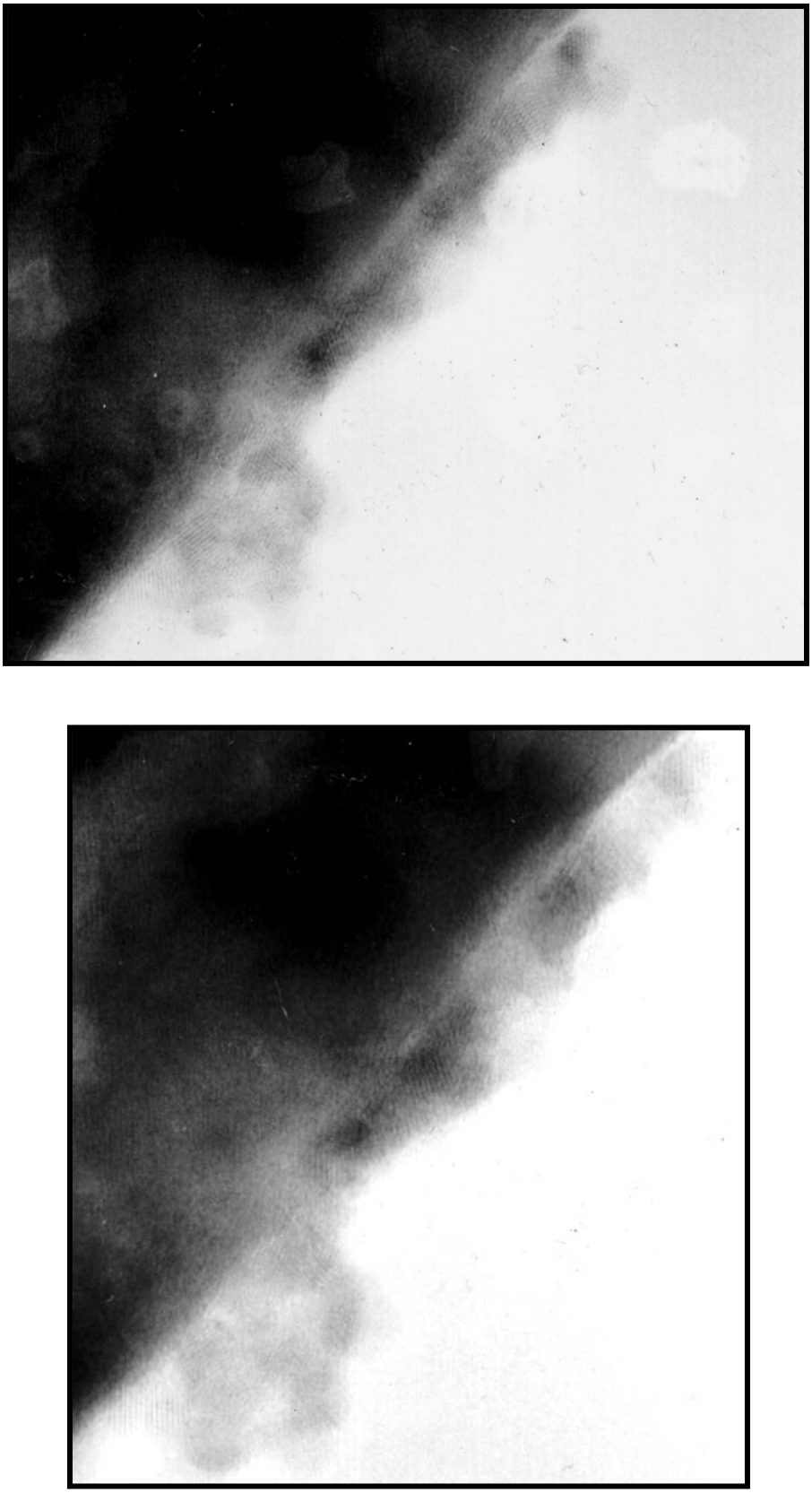

Figure 16. TEM Micrographs of nanocrystals on the surface of TiO_2

A word on imaging the nanotube-nanocrystal composite structure. The system has proven difficult to image for a number of reasons. One, the mass contrast difference between TiO_2 and CdSe makes it difficult to pick out the CdSe nanocrystals. Two, when the CdSe is attached to anatase-TiO_2 nanotubes, the fringe patterns overlap and prove difficult to identify. One solution to this was to skip the anneal stage of the anodization, and link nanocrystals to amorphous TiO_2 samples. This proved to be a helpful technique, if only for imaging purposes. Three, it is difficult to get a sense of the uniformity of coverage in the TEM. Nanocrystals bound to the nanotube surface can be seen only in profile, with no indication of the depth of coverage.

6.4.3. Electrophoretic Deposition

EPD was also successful in depositing nanocrystals onto the TiO_2 surface, as can be seen from the EDS spectrum collected in Figure 17. Quantitative data associated with the EDS output is provided in Table 3, indicating the presence of CdSe on the surface. While EPD presents an impressive alternative to the lengthy process of chemical linking, we have found it limited in that the success of a deposition is highly dependant on the quality and cleanliness of the nanocrystal sample to be deposited. At this point in time, more work is necessary to understand the kinetics of the EPD process to make it a viable option for a wider range of nanocrystal preparations.

Element	Spect. Type	Element %	Atomic %
O	ED	52.90	77.39
Ti	ED	45.35	22.16
Se	ED	0.94	0.28
Cd	ED	0.81	0.17
Total		100.00	100.00

Table 3: EDS Quantitative Composition Data for EPD deposition

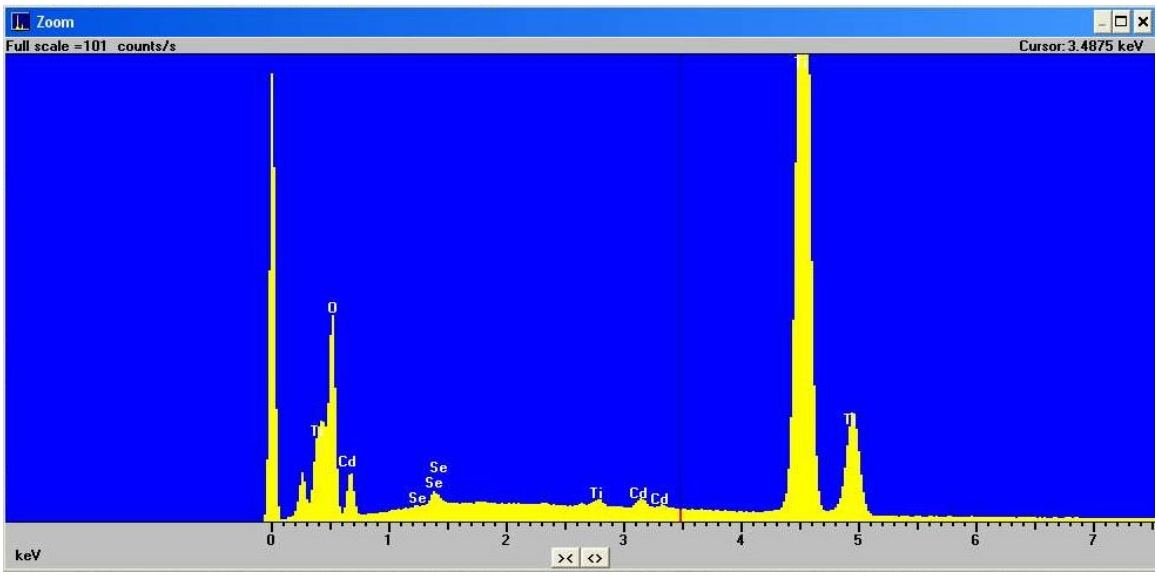

Figure 17. EDS Spectra for nanocrystals deposited on TiO2 via EPD

7. Conclusions and Future Work

While this project did not successfully produce a working photovoltaic device, significant progress has been made in the individual components of the system. This thesis describes two of those components: fabrication of an ordered TiO_2 thin film as electron conducting layer, and deposition of nanocrystals onto the TiO_2surface. The anodized titanium nanotubes are a significant improvement over the earlier template technique. Additionally, electrophoretic deposition presents a novel approach to nanocrystal deposition techniques and is a promising alternative to the current chemical linking procedure. However, significant new approaches to imaging the deposited nanocrystals must be developed to verify surface coverage by these deposition techniques, particularly due to the highly ordered structure of the TiO_2 thin films. Future work will be directed at completing the solar cell device by depositing a hole conducting layer on top of the nanotube array. Nanocrystal-sensitized solar cells may soon prove to be viable alternative to silicon photovoltaics.

References

[1] **Campbell, C.J. and J.H. Laherrere, "The end of cheap oil".** ***Scientific American,*** **1998. 278(3): p. 60-5.**

[2] **Goh, C., K.M. Coakley, and M.D. McGehee, "Nanostructuring titania by embossing with polymer molds made from anodic alumina templates".** ***Nano Lett,*** **2005. 5(8): p. 1545-1549.**

[3] **Kippeny, T., L.A. Swafford, and S.J. Rosenthal, "Semiconductor Nanocrystals: A Powerful Visual Aid for Introducing the Particle in a Box".** ***Journal of Chemical Education,*** **2002. 79(9): p. 1094-1094.**

[4] ***Climate Change 2007: The Physical Science Basis - Summary for Policy Makers,*** **I.P.o.C. Change, Editor. 2007.**

[5] **Swafford, L.,** ***Homogeneously Alloyed Cadmium Sulfoselenide Nanocrystals.*** **2006, Vanderbilt University: Nashville.**

[6] **Smalley, R.E., "Future Global Energy Prosperity: The Terawatt Challenge".** ***MRS BULLETIN,*** **2005. 30: p. 413-413.**

[7] **Lewis, N.S. and G. Crabtree, "Basic Research Needs for Solar Energy Utilization".** ***Report on the Basic Energy Sciences Workshop on Solar Energy Utilization, Office of Science, US Department of Energy, Washington, DC,*** **2005.**

[8] **Colvin, V.L., M.C. Schlamp, and A.P. Alivisatos, "Light-emitting diodes made from cadmium selenide nanocrystals and a semiconducting polymer".** ***Nature,*** **1994. 370(6488): p. 354-357.**

[9] **Gao, M., et al., "Electroluminescence of different colors from polycation/CdTe nanocrystal self-assembled films". *Journal of Applied Physics*, 2000. 87: p. 2297-2297.**

[10] **Bowers, M.J., J.R. McBride, and S.J. Rosenthal, "White-light emission from magic-sized cadmium selenide nanocrystals". *Journal of the American Chemical Society*, 2005. 127(44): p. 15378-15379.**

[11] **Swafford, L.A., et al., *Molecular and Nanomaterial-Based Photovoltaics*, in *Molecular Nanoelectronics*. 2003, American Scientific Publishers.**

[12] **Erwin, M.M., et al., "Material characterization of a nanocrystal based photovoltaic device". *The European Physical Journal D-Atomic, Molecular and Optical Physics*, 2001. 16(1): p. 275-277.**

[13] **Greenham, N.C., X. Peng, and A.P. Alivisatos, "Charge separation and transport in conjugated-polymer/semiconductor-nanocrystal composites studied by photoluminescence quenching and photoconductivity". *Physical Review B*, 1996. 54(24): p. 17628-17637.**

[14] **Schaller, R.D. and V.I. Klimov, "High Efficiency Carrier Multiplication in PbSe Nanocrystals: Implications for Solar Energy Conversion". *Physical Review Letters*, 2004. 92(18): p. 186601-186601.**

[15] **Klein, D.L., et al., "A single-electron transistor made from a cadmium selenide nanocrystal". *Nature*, 1997. 389(6652): p. 699-699.**

[16] **Rosenthal, S.J., et al., "Targeting cell surface receptors with ligand-conjugated nanocrystals". *Journal of the American Chemical Society*, 2002. 124(17): p. 4586-4594.**

[17] **Medintz, I.L., et al., "Quantum dot bioconjugates for imaging, labelling and sensing". *Nat Mater*, 2005. 4(6): p. 435-46.**

[18] **Chan, W.C.W. and S. Nie, "Quantum Dot Bioconjugates for Ultrasensitive Nonisotopic Detection". *Science*, 1998. 281(5385): p. 2016-2016.**

[19] **Alivisatos, A.P., "Perspectives on the Physical Chemistry of Semiconductor Nanocrystals". *J. Phys. Chem*, 1996. 100(31): p. 13226-13239.**

[20] **Ekimov, A.I., et al., "Absorption and Intensity-Dependent Photoluminescence Measurements on Cdse Quantum Dots-Assignment of the 1st Electronic-Transitions". *Journal of the Optical Society of America B-Optical Physics*, 1993. 10: p. 100-107.**

[21] **Brus, L.E., "A simple model for the ionization potential, electron affinity, and aqueous redox potentials of small semiconductor crystallites". *The Journal of Chemical Physics*, 1983. 79: p. 5566-5566.**

[22] **Brus, L.E., "Electron-electron and electron-hole interactions in small semiconductor crystallites: The size dependence of the lowest excited electronic state". *The Journal of Chemical Physics*, 1984. 80: p. 4403-4403.**

[23] **Green, M.A., "Solar cells: Operating principles, technology, and system applications". *Englewood Cliffs, NJ, Prentice-Hall, Inc., 1982. 288 p.*, 1982.**

[24] **Shockley, W. and H.J. Queisser, "Detailed Balance Limit of Efficiency of pn Junction Solar Cells". *Journal of Applied Physics*, 1961. 32: p. 510-519.**

[25] **O'Reagan, B. and M. Grätzel, "A low-cost, high-efficiency solar cell based on dye-sensitized colloidal TiO 2 films". *Nature*, 1991. 353: p. 737-740.**

[26] **Grätzel, M., "Dye-sensitized solar cells". *Journal of Photochemistry & Photobiology, C: Photochemistry Reviews*, 2003. 4(2): p. 145-153.**

[27] **Nazeeruddin, M.K., et al., "Engineering of efficient panchromatic sensitizers for nanocrystalline TiO 2-based solar cells". *J. Am. Chem. Soc*, 2001. 123(8): p. 1613-1624.**

[28] **Schmidt-Mende, L., S.M. Zakeeruddin, and M. Grätzel, "Efficiency improvement in solid-state-dye-sensitized photovoltaics with an amphiphilic Ruthenium-dye". *Applied Physics Letters*, 2004. 86: p. 013504-013504.**

[29] **Peter, L.M., et al., "Photosensitization of nanocrystalline TiO 2 by self-assembled layers of CdS quantum dots". *Chemical Communications*, 2002. 2002(10): p. 1030-1031.**

[30] **Robel, I., et al., "Quantum Dot Solar Cells. Harvesting Light Energy with CdSe Nanocrystals Molecularly Linked to Mesoscopic TiO2 Films". *Journal of the American Chemical Society*, 2006. 128(7): p. 2385-2393.**

[31] **Nozik, A.J., "Quantum dot solar cells". *Physica E: Low-dimensional Systems and Nanostructures*, 2002. 14(1-2): p. 115-120.**

[32] **Wijayantha, K.G.U., L.M. Peter, and L.C. Otley, "Fabrication of CdS quantum dot sensitized solar cells via a pressing route". *Solar Energy Materials and Solar Cells*, 2004. 83(4): p. 363-369.**

[33] **Macak, J.M., et al., "Smooth anodic TiO2 nanotubes: annealing and structure". *Physica Status Solidi A*, 2006. 203(10): p. 67-9.**

[34] Tsuchiya, H., et al., "Self-organized TiO2 nanotubes prepared in ammonium fluoride containing acetic acid electrolytes". *Electrochemistry Communications*, 2005. 7(6): p. 576-80.

[35] Yoriya, S., et al., "Fabrication of vertically oriented TiO2 nanotube arrays using dimethyl sulfoxide electrolytes". *Journal of Physical Chemistry C*, 2007. 111(37): p. 13770-6.

[36] Qingyun, C., et al., "The effect of electrolyte composition on the fabrication of self-organized titanium oxide nanotube arrays by anodic oxidation". *Journal of Materials Research*, 2005. 20(1): p. 230-6.

[37] Shankar, K., et al., "Highly-ordered TiO2 nanotube arrays up to 220 ?m in length: use in water photoelectrolysis and dye-sensitized solar cells". *Nanotechnology*, 2007. 18(6): p. 11 pp.-11 pp.

[38] Chu, S.Z., et al., "Highly porous (TiO2-SiO2-TeO2)/Al2O3/TiO2 composite nanostructures on glass with enhanced photocatalysis fabricated by anodization and sol-gel process". *Journal of Physical Chemistry B*, 2003. 107(27): p. 6586-6589.

[39] Paulose, M., et al., "Unprecedented ultra-high hydrogen gas sensitivity in undoped titania nanotubes". *Nanotechnology*, 2006. 17(2): p. 398-402.

[40] Prakasam, H.E., et al., "A new benchmark for TiO2 nanotube array growth by anodization". *Journal of Physical Chemistry C*, 2007. 111(20): p. 7235-41.

[41] Murray, C.B., D.J. Norris, and M.G. Bawendi, "Synthesis and characterization of nearly monodisperse CdE (E= sulfur, selenium, tellurium)

semiconductor nanocrystallites". *Journal of the American Chemical Society*, 1993. 115(19): p. 8706-8715.

[42] Peng, X., J. Wickham, and A.P. Alivisatos, "Kinetics of II-VI and III-V Colloidal Semiconductor Nanocrystal Growth:'Focusing'of size distributions". *Journal of the American Chemical Society*, 1998. 120(21).

[43] Yu, W.W., et al., "Experimental determination of the extinction coefficient of CdTe, CdSe, and CdS nanocrystals". *Chem. Mater*, 2003. 15(14): p. 2854-2860.

[44] Lawless, D., S. Kapoor, and D. Meisel, "Bifunctional Capping of CdS Nanoparticles and Bridging to TiO2". *The Journal of Physical Chemistry*, 1995. 99(25): p. 10329-10335.

[45] Shim, M. and P. Guyot-Sionnest, "Permanent dipole moment and charges in colloidal semiconductor quantum dots". *Journal of Chemical Physics*, 1999. 111: p. 6955-6964.

[46] Besra, L. and M. Liu, "A review on fundamentals and applications of electrophoretic deposition (EPD)". *Progress in Materials Science*, 2007. 52(1): p. 1-61.

[47] Goldstein, J., et al., *Scanning Electron Microscopy and X-ray Microanalysis*. 2003: Springer. 689.

[48] Williams, D.B. and C.B. Carter, *Transmission Electron Microscopy: A Textbook for Materials Science*. 1996: Springer.

[49] Feldman, L.C. and J.W. Mayer, *Fundamentals of Surface and Thin Film Analysis*. 1986: North Holland-Elsevier.

[50] **Grimes, C.A., et al., "A review on highly ordered, vertically oriented TiO2 nanotube arrays: Fabrication, material properties, and solar energy applications". *Solar Energy Materials and Solar Cells*, 2006. 90(14): p. 2011-75.**

[51] **Mor, G.K., et al., "Transparent highly ordered TiO2 nanotube arrays via anodization of titanium thin films". *Advanced Functional Materials*, 2005. 15(8): p. 1291-6.**